LUND UNIVERSITY
Faculty of Science

Getting more from LEED: The implementation and possibilities of spatially resolved mapping

Valter Sundström

Thesis submitted for the degree of Bachelor of Science
Project duration: 2 months

Supervised by Craig Polley and Joachim Schnadt

Department of Physics
Division of Synchrotron Radiation Research
May 2024

Acknowledgements

Above all, I am forever grateful to my wife, **Vedrana Pavlak**, for supporting me throughout my studies and being my best friend, enabling me to reach the point of completion of this project. I must also express immense gratitude towards **Craig Polley** for being my project companion and mentor throughout this study, and **Joachim Schnadt** for his support and insight when putting this document together. At each step where I have felt confusion or lack of understanding, support has always been available, through their clear and efficient communication, knowledge, and willingness to make time for me and my questions. Additionally, I thank everyone in the **Bloch beamline team** at the MAX IV Laboratory, where I have felt very welcome and at home. Special thanks goes to **Jacek Osiecki** who has supported me during LEED experiments, in practical matters as well as being a conversation partner willing to engage with my questions, helping me understand what I am doing and how things work.

Abstract

We extend the capabilities of a LEED instrument to allow raster scanning across entire samples, giving a map of LEED patterns. The method gives a macroscopic view of the inhomogeneity and quality of samples, and we propose that the usage of LEED scanning as a simple alternative to more complex methods has viable uses during sample preparation, without the need for costly beamtime. Results from inhomogeneity mapping of a monolayer SiC sample were compared to scans taken with photoemission spectroscopy, showing good agreement. The photoemission measurements took ten times longer to perform and required significantly more advanced practical knowledge. Additionally, a badly cleaved sample of $PtTe_2$ was investigated, allowing the localization of miniscule LEED patterns by analysing raster scans.

Popular science summary

Human interest in materials science is as old as civilization itself. What has changed dramatically is the number of different specialized materials we now require, and the complexity of producing and researching them. For extreme performance in heat and energy conduction, as well as other unique properties, we must work at the smallest scale in the relatively new field of nanotechnology, born in the 1980s. Materials where one dimension is on the nanoscale, meaning we have an extremely thin sheet of something rather than a three-dimensional crystal, are called 2D materials or simply nanosheets. Graphite is a material commonly encountered in the form of pencils, and it is made up of nanosheets of graphene. Graphene was successfully isolated in 2004, becoming the first in a new wave of exfoliable 2D materials, and along with superb electrical and thermal conductivity it is currently the mechanically strongest material ever tested.

At the nano-scale, the equipment needed for research becomes highly complex and often very energy intensive. Some technologies allow us to explore material surfaces with fewer resources, such as Scanning Tunneling Microscopy (STM) or Low Energy Electron Diffraction (LEED), but for detailed investigation of material properties, usage of high-energy beams is often required. This either means access to large and expensive lasers, or particle accelerators, of which there are relatively few in the world with long waiting lines and strict selection processes. There simply isn't enough beamtime for everyone who could use it. In light of this situation we would benefit from maximizing the usage of simpler and more accessible tools. By way of example, here we demonstrate how low energy electron diffraction (LEED) can be extended to provide richer insights during sample preparation procedures. A sample can be extremely small, or the surface can be inhomogeneous or hard to clean, making it difficult and time consuming to find good measurement spots. LEED is an especially surface sensitive technique that tells us about the crystal structure at a point on a sample, and it is a simple, common and relatively inexpensive technique available to any lab that needs it. By taking LEED measurements across a whole sample, we can observe subtle variations in crystal ordering or quality, and pinpoint the best measurement spots or find potential preparation issues. This allows for better preparation before gaining access to a beamline or other facility with time limitations, in order to make the most out of the time allotted there.

Contents

1 Introduction **2**

1.1 SiC monolayer on TaC . . . 3

1.2 $PtTe_2$ . . . 4

2 Background **5**

2.1 Low Energy Electron Diffraction (LEED) . . . 5

2.1.1 Scattering . . . 6

2.2 Low Energy Electron Diffraction (LEED) apparatus . . . 7

2.3 2D raster scanning . . . 8

2.4 Photoemission spectroscopy: XPS and ARPES . . . 8

3 Experimental setup **10**

4 Method and development **11**

4.1 Sample preparation . . . 12

4.2 Extension of existing Low Energy Electron Diffraction (LEED) capabilities 13

4.3 Analysis . . . 14

5 Results: SiC on TaC and small crystal cleaving **15**

5.1 SiC on TaC . . . 15

5.1.1 Graphene layers . . . 15

5.1.2 Inhomogeneity of monolayer SiC . . . 18

5.2 Small crystal ($PtTe_2$) . . . 19

5.3 Multiple cleaved samples . . . 21

6 Conclusion **22**

7 Outlook **23**

Acronyms

ARPES Angle-Resolved Photoemission Spectroscopy

LEED Low Energy Electron Diffraction

PEEM Photo-Emission Electron Microscopy

PES Photoelectron Spectroscopy

SiC silicon carbide

TaC tantalum carbide

UHV Ultra-High Vacuum

XPS X-ray Photoelectron Spectroscopy

1 Introduction

Human interest in materials science is as old as civilization itself, and today modern advancements in technology and scientific understanding allow exploration of physical structures at atomic level, as well as manipulation at the nanoscale. When one or several axes of a crystal structure are on this scale, the material effectively has fewer structural dimensions. In the case where a single dimension is removed, one has a 2D material, commonly referred to as a nanosheet. Such a sheet can be formed from a single layer of atoms and is then referred to as a monolayer 2D material. One can also have 1D nanowires or 0D nanodots, which are relevant for many use cases but will not be the focus of this study. The first in a new wave of exfoliable 2D materials is graphene, initially isolated by Konstantin Novoselov and Andre Geim in 2004 [1]. The importance of their achievement is highlighted by the Nobel Prize awarded for their work in 2010 [2], and the explosion of research into nanomaterials since then. In this study, the usage of Low Energy Electron Diffraction (LEED) is explored as a tool for investigating the quality and homogeneity of samples by taking raster scans across entire sample areas. The results are shown to be comparable with measurements attained from the more advanced technique of Angle-Resolved Photoemission Spectroscopy (ARPES), with much less investment in time and complexity. The study was performed at the Bloch beamline at the MAX IV Laboratory, and the inhomogeneity of a monolayer silicon carbide (SiC) sample grown on tantalum carbide (TaC) was investigated. This sample had been grown previously in the course of another ARPES study at Bloch [3]. Further, the quality of surface structures was explored using a cleaved crystal of $PtTe_2$, as well as an array of four cleaved crystals in a single sample holder. The latter example mirrors a situation where a scientist may be using samples which rarely present a well-ordered surface structure when cleaved. Chances can be increased by cleaving several crystals on a single holder, which can be a very time-consuming process, but one is then faced with the challenge of identifying well-cleaved samples and locating where they are on the holder. An extreme real-world example of this approach can be seen in Fig. 1, where 15 crystals of the same type were mounted on a single holder. In the following sections, we briefly discuss the two types of samples used in this study in more detail.

FIG. 1: Example of several samples mounted on a single holder for an ARPES experiment. Each crystal (not fully visible) is glued onto a copper plate together with a ceramic rod which facilitates cleaving inside a vacuum chamber. By pushing the rods, the crystals cleave and a pristine surface is exposed within the vacuum environment. The cleaving process does not always produce useful surfaces, often necessitating multiple attempts. The figure shows an example of a particularly difficult case, where 15 identical crystals were mounted on a single holder.

1.1 SiC monolayer on TaC

Similarily to graphene, monolayer SiC also forms a honeycomb structure, and there is strong DFT-based theoretical support for expectations of interesting optical and electrical properties. Calculations predict a direct band-gap of around 2.5 eV [4], making SiC suitable for optoelectronic applications [5]. Notably, this applies specifically to monolayer SiC, but not multilayer 2D-SiC, where the band gap is indirect. The properties of planar SiC have been studied extensively and show strong support for optoelectronic and electronic applications as well as chemical sensing [6]. A large and tunable band gap makes it specifically interesting for light-emitting devices and solar cells.

Given these properties, there has been significant interest in synthesizing large sheets of monolayer SiC, which has proven challenging. Unlike graphene, 2D-SiC does not exist as a layered bulk material, and until recently successful synthesis was restricted to nanoflakes [7]. However, a recent paper published in collaboration with the team at the Bloch beamline has shown that large-scale 2D-SiC can be grown on top of thin films of TaC or NbC on a SiC substrate [3]. A graphic of the sample is shown in Fig. 2. For our study, which was also performed at the Bloch beamline, the same SiC-on-TaC sample was

investigated using LEED raster scans for the purpose of imaging surface inhomogeneity. The primary expectation was to find graphene around the edges of the sample, as the preparation process of the sample means there is no TaC layer there, and the process of SiC turning into graphene during annealing is by now well understood.

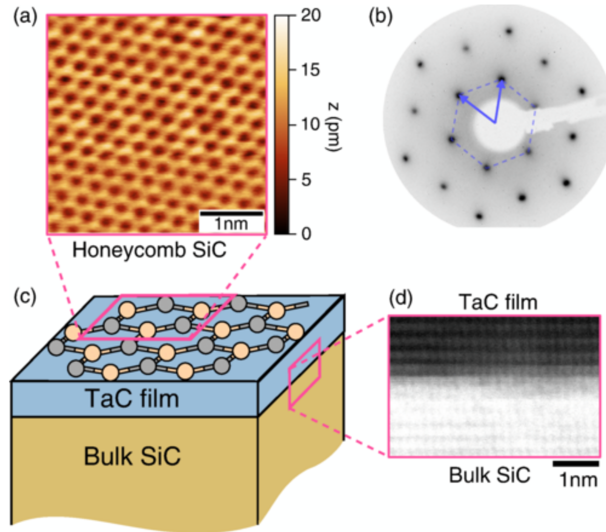

FIG. 2: Depiction of the sample used by Polley *et al.* for growing monolayer SiC on top of TaC, featuring imaging with (a) scanning tunnelling microscopy (STM,) (b) LEED and (d) High-Angular Dark-Field Scanning Transmission Electron Microscopy [3].

1.2 $PtTe_2$

Platinum ditelluride ($PtTe_2$) is part of the group of transition metal dichalcogenides (TMDs), which consist of layers of transition metal atoms in-between chalcogens. Similarily to the layered nature of graphite, TMDs are also layered materials, with the layers held together by van der Waals-forces. The layers can be easily exfoliated, and as with other 2D materials they exhibit interesting electronic properties when thickness is reduced. Prior studies have shown that, as the TMD thickness is reduced to monolayer, the indirect band gap present in the bulk changes into a direct one [8]. This makes $PtTe_2$ viable for semi-conductor [9] and photoelectronic applications, such as mid-infrared photodetection [10]. 2D materials that can be grown as wafer-scale crystals, such as $PtTe_2$, are often experimentally investigated by cleaving a crystal and probing using a surface-sensitive technique. During cleaving, a well-formed surface structure may or may not present itself, and the difficulty of attaining a useable sample varies depending on the

crystal. In this study, a $PtTe_2$ crystal was cleaved and the best measurement area was localized using LEED raster scanning.

2 Background

2.1 Low Energy Electron Diffraction (LEED)

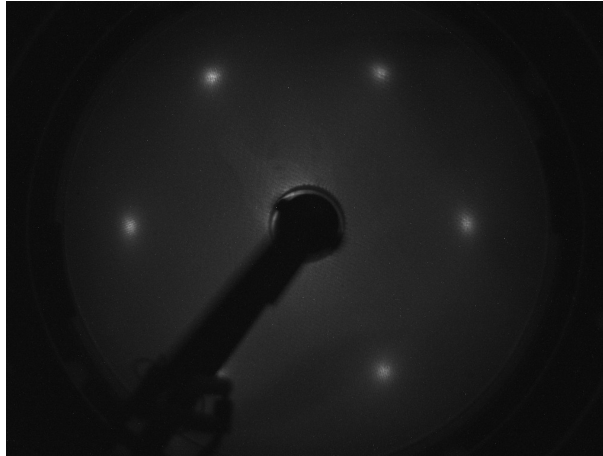

FIG. 3: LEED pattern of monolayer SiC. The bright spots stem from constructive interference of low-energy electrons which have scattered from the sample surface. The arrangement of the spots, as well as their shape and intensity, gives useful information about the structural ordering at the surface.

LEED is a method for observing the crystal structure of material surfaces by measuring the backscattering of electrons. It exploits the wavelike behaviour of electrons, causing interference patterns as seen in Fig. 3, where the bright points represent peaks of constructive interference. Electrons are accelerated to energies of 20 eV to 1000 eV, giving rise to the term "Low energy" in relation to high-energy techniques such as X-ray diffraction. This makes the method highly surface-sensitive, as electrons in this energy range undergoing inelastic scattering have a mean free path length in the range of 5 Å to 20 Å [11], which is on the magnitude of a few atomic layers. The main reason this energy range is chosen, however, becomes apparent when the de Broglie-wavelength for such particles is calculated. For electron energies of 20 eV to 1000 eV, one gets wavelengths of 2.74 Å to 0.388 Å [11]. When compared to the interatomic spacing in, for example, diamond of ∼1.54 Å, it becomes apparent that such electron beams can diffract upon interaction

with a periodically arranged surface of atoms, allowing the production of so-called LEED patterns.

2.1.1 Scattering

To understand how the pattern in Fig. 3 is produced, the one-dimensional case is first explored, where a monochromatic electron beam is aimed orthogonally onto an array of evenly spaced atoms. Scattering will occur at each atom and the incident electron beam will be back-scattered with some angle θ dependent on the lattice constant a. The difference in path length for beams from each scattering point is given by $a \sin\theta$, which means that for constructive interference one has the condition

$$a \sin\theta = n\lambda, \tag{1}$$

where λ is the fixed wavelength of the electron beam and n is an integer.

Using the de Broglie relation

$$\lambda = \frac{h}{p}, \tag{2}$$

and expressing the momentum in terms of the wavevector $\boldsymbol{k_0}$ of the incident beam, one can rewrite (1) as

$$a \sin\theta = n\frac{2\pi}{k_0}, \tag{3}$$

or, equivalently,

$$k_0 \sin\theta = \Delta k_{||} = n\frac{2\pi}{a}. \tag{4}$$

This now gives the condition for constructive interference in terms of the parallel momentum of scattered electrons relative the target array. Given that the wavevector is of dimension reciprocal length, the array constructed by equation (4) is called the reciprocal lattice vector, which quantizes the parallel momentum exchange with the target at interference peaks.

Repeating the argument in two dimensions with a line spacing of b, one can define the following rules for the two-dimensional reciprocal unit vectors

$$\boldsymbol{a}^* = \frac{2\pi}{\boldsymbol{a}} \tag{5}$$

$$\boldsymbol{b}^* = \frac{2\pi}{\boldsymbol{b}} \tag{6}$$

$$\boldsymbol{a} \cdot \boldsymbol{b}^* = \boldsymbol{b} \cdot \boldsymbol{a}^* = 0, \tag{7}$$

where **a** and **b** are the unit vectors in real space of the surface unit cell. The reciprocal lattice vector can then be defined as

$$\boldsymbol{G} = n\boldsymbol{a}^* + m\boldsymbol{b}^*, \tag{8}$$

where n and m are integers, as before. The reciprocal lattice vector forms the basis of observed LEED patterns, and by converting them back from reciprocal space into real space one gets a measurement of the symmetries in the crystal lattice.

2.2 LEED apparatus

As introduced in the previous section, the main components needed for a LEED experiment are an electron gun to produce the low-energy electrons, a sample, and some way of observing the scattered electrons. Such a setup, where a fluorescent screen plays the part of the detector, is depicted in Fig. 4, but it also includes a few extra considerations. In order for accurate measurements to be taken, the electron beam must be undisturbed and only elastically scattered electrons should reach the screen. To this end, the experiment is performed in ultrahigh vacuum and the apparatus ensures that no electromagnetic fields disturb the electron paths. In Fig. 4, four grids are visible in front of the screen. The outer and inner grids are grounded to ensure the electrons move without field interference. In between the grounded grids are two negatively biased grids acting as filters, preventing non-elastically scattered electrons from being measured. Finally, the screen itself is positively biased in order to accelerate electrons enough for a fluorescent response.

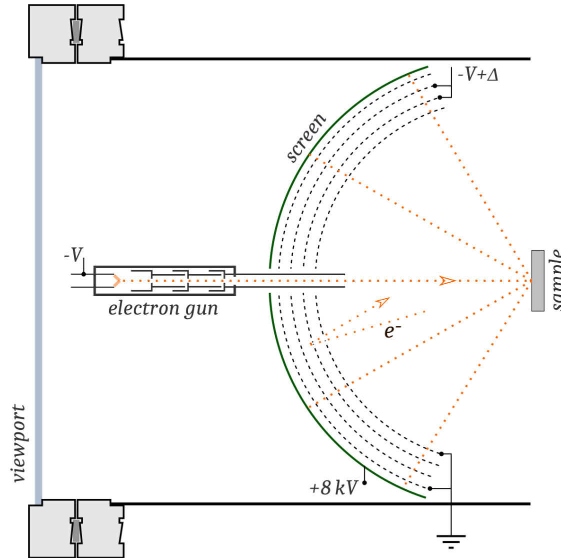

FIG. 4: Example schematic of LEED setup [12]. An electron gun is pointed orthogonally onto a sample. The electron beam diffracts on the sample and travels towards a semi-spherical fluorescent screen. In front of the screen, non-elastically scattered electrons are rejected by a filtering mechanism. Finally, the remaining elastically scattered electrons are accelerated by high voltage towards the screen to trigger a fluorescent response which produces an observable LEED pattern.

2.3 2D raster scanning

In the common case, LEED measurements are taken at a single location of a sample, giving information about the structure of the lattice at that particular point. For well-formed homogeneous crystals, a location with a clear LEED pattern can easily be found through small movements across the sample, but often this is not the case. Samples may have small areas of well-formed surface structure, areas of inhomogeneity, or other aspects making the use of LEED or other surface-sensitive techniques difficult. There may also be useful information which can only be gained from an overview of the LEED behaviour across the entire sample. In this study, a few such cases will be investigated through the use of LEED raster scanning.

2.4 Photoemission spectroscopy: XPS and ARPES

Photoelectron Spectroscopy (PES) is a group of experimental techniques for investigating the electronic properties of materials, based on the photoelectric effect. Compared with LEED, where an external electron beam is used to probe the sample, PES instead measures

the energies of the electrons bound in the solid by probing with photons. The photoelectric effect tells us that if an incoming photon is energetic enough, an electron will be kicked out at an angle ϑ with respect to the surface normal, carrying a kinetic energy of

$$E_k = h\nu - \phi - E_B, \tag{9}$$

where ν is the frequency of the photon, ϕ is the work function of the analyzer and E_b is the electron binding energy. The work function is the energy needed for an electron in the material at Fermi level to escape the material into vacuum [13]. Photoemission spectroscopy where X-rays are used, and the kinetic energy of emitted core electrons is measured, is called X-ray Photoelectron Spectroscopy (XPS). The energy of core electrons is a result of their related nucleus, but also of the binding environment of the atom, hence XPS is well suited for exploration of chemical structure. A more advanced technique, where both kinetic energy and emission angle of valence electrons is measured is called ARPES. A schematic of an ARPES setup can be seen in Fig. 5 and Fig. 6. During photoemission, the parallel momentum $\mathbf{k}_{||}$ is conserved, while this is not true for the perpendicular momentum [14], since transfer through the material surface breaks translational symmetry in the perpendicular direction. From the conservation of parallel momentum the following relation can be derived:

$$\hbar k_{||} = \sqrt{2mE_{kin}} \sin\vartheta, \tag{10}$$

where $\hbar k_{||}$ is the parallel crystal momentum of an electron emitted at angle ϑ [15]. By measuring ϑ and E_{kin} using ARPES, one can then use equation (10) to find the conserved momentum $\mathbf{k}_{||}$ of the emitted electrons, which is directly correlated to the energy bands available in a material. The measured kinetic energy E_{kin} is dependent on the energy $h\nu$ used during the experiment, and plotted data is therefore generally presented in terms of the binding energy E_b, given by

$$E - E_F = -E_b, \tag{11}$$

where E_F is the Fermi level of the sample [15].

In summary, XPS gives a direct measurement of the binding energy levels of core electrons, from which the chemical structure can be determined. ARPES additionally measures the emission angle, allowing exploration of the band structure, which gives significant insight into the electronic properties of materials.

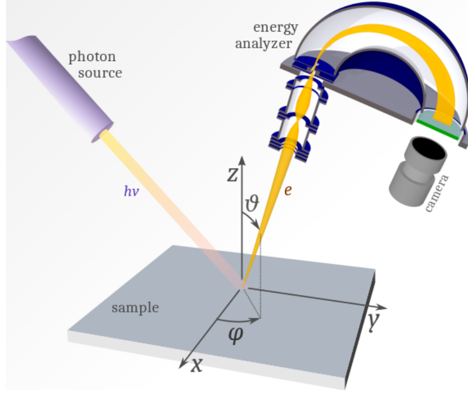

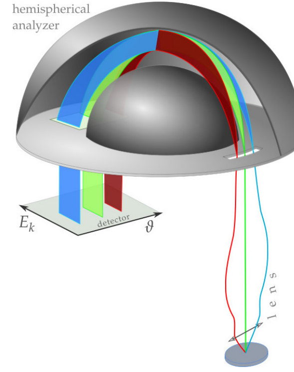

FIG. 5: Schematic of ARPES experimental setup [16]. A photon source is aimed onto a surface, and electrons are emitted from the surface at an angle ϑ along the y-axis. The electrons are captured into an analyzer where the angle of emission and their kinetic energy is measured.

FIG. 6: Schematic of a hemispherical energy analyzer, commonly used in ARPES experiments [17]. A narrow electrostatic lens initially amplifies the angular spread of incoming electrons, before they are dispersed onto a detector where the kinetic energy and emission angle is recorded.

3 Experimental setup

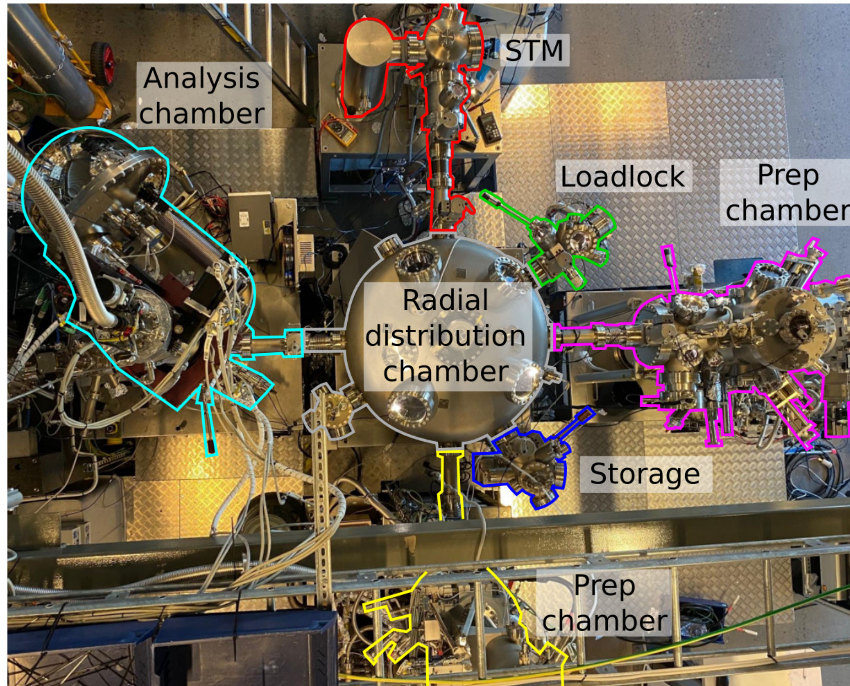

FIG. 7: Overview of A-branch endstation at the Bloch beamline. A total of 7 Ultra-High Vacuum (UHV) chambers house the main ARPES instrument, STM, two prep chambers with LEED instruments, sample storage and loadlock [18]. The prep chamber marked in yellow was used for this study.

The experiments for this study were conducted at the Bloch beamline at the MAX IV Laboratory in Lund, Sweden. The station mainly focuses on ARPES but is designed with flexibility in mind. To this end it contains a Scanning Tunneling Microscope (STM) and two prep chambers equipped with LEED instruments, as seen in Fig. 7. This allows users to prepare and investigate samples using different methods before using the beamline, without ever having to leave the Ultra-High Vacuum (UHV) chambers. In this study the prep chamber marked in yellow was used, where the functionality of the LEED and motor controls were extended to allow for raster scanning.

4 Method and development

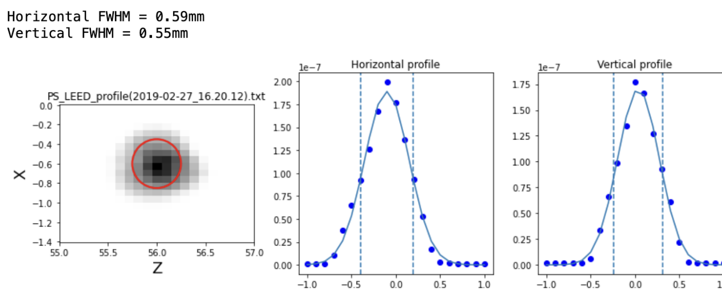

FIG. 8: Representative measurement of LEED spot size, showing a spatially resolved profile of beam current convolved through a 500 µm aperture. The measurements were taken with the LEED instrument at the Bloch beamline, which has since had the electron gun replaced. Hence, the data is not fully accurate for the current study, but gives a sense of what resolution can be expected.

Three different samples were chosen based on expected characteristics motivating usage of LEED scans, rather than measurements at individual points. TaC was chosen with strong expectation of inhomogeneous surface reconstruction. A $PtTe_2$ crystal was cleaved inside the LEED chamber as an example of finding optimal measurement spots on a sample where only a small area may have cleaved well. Lastly, multiple arbitrary crystals were cleaved on a single sample holder inside the chamber in an attempt to identify how many and how well each had cleaved. Cleaving was performed by top posting, meaning a small stick was glued onto the samples prior to transfer into the chamber, as seen in Fig. 1. The stick was then gently pushed, while inside the chamber, until the sample cracked. LEED raster scans were taken for each sample, using custom software for control of the scanning

process. For the SiC-on-TaC sample, a supplementary ARPES scan was performed. The results were analyzed using existing software, originally developed at the Bloch beamline for ARPES raster scans.

An important characteristic for the validity of using a LEED instrument as a raster scanning device is the spot size. A large spot size, on the order of millimeters, would invalidate the utility of spatially resolved LEED maps, as the observed diffraction patterns is an average over all probed regions and hence the spatial resolution would be very low. An old measurement of the instrument used during this study is presented in Fig. 8. The electron gun has been replaced after the measurement was taken, but as the replacement is expected to be equivalent, the previous results are assumed to still be valid. The spot size was investigated using a special sample, which measured the beam current through a pinhole aperture of approximately 500 µm radius, while being raster scanned through the beam. The result in Fig. 8 shows a spot size of 0.5 mm to 0.6 mm, which is close to the size of the aperture. It is therefore reasonable to assume the resolution of the measurement is limited by the aperture size, and represents an upper limit of the spot size, rather than the true value.

4.1 Sample preparation

The first used sample was prepared as part of the study of growing monolayer SiC on TaC [3]. Part of the process included annealing, which was not entirely uniform and can be observed in Fig. 11a. The full surface of the sample was not covered by the TaC film, leaving an edge of exposed bulk SiC. Because of this, there is a strong expectation that graphene formed along the edges during annealing.

The second sample, a $PtTe_2$ crystal, was glued onto the centre of a sample holder, top posted, and cleaved inside the preparation chamber in UHV just before being put in front of the LEED instrument. For the multiple samples on a single holder, seen in Fig. 9, a similar process was repeated. In this case the crystals were evenly spaced horizontally along the centre of the sample holder and top posted in preparation for in-chamber cleaving.

FIG. 9: Four arbitrary crystals mounted on a single holder and cleaved inside UHV. The picture was taken after the measurements were performed and the sample had been removed from the chamber.

4.2 Extension of existing LEED capabilities

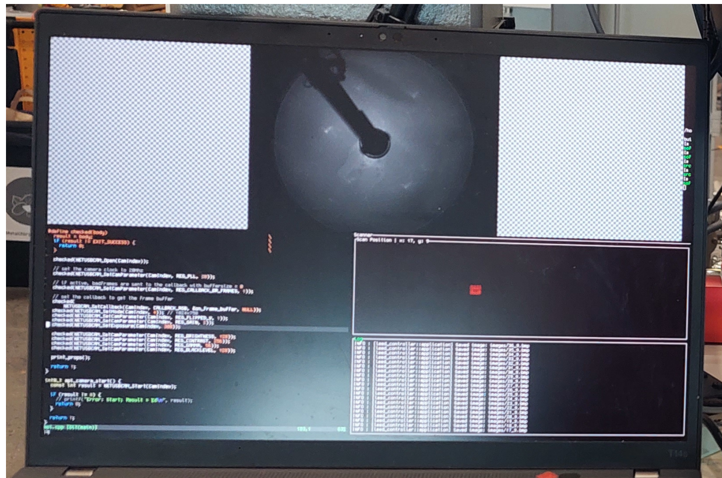

FIG. 10: LEED scan in progress using software developed during the study. A live feed of the LEED camera is visible in the upper part of the screen. The lower right corner displays the current scan position, as well as a log of saved images and other messages.

The standard procedure when taking LEED measurements consists of manually dialling in LEED settings using a software or hardware controller, then using a different interface for mechanically moving the sample into position, and finally saving images of good patterns. This is also how the setup at the Bloch beamline is commonly operated. A raster scan can be performed by a user in this manner, and it is often the case that one moves across a sample until a good location is found. There are obvious downsides to this type of manual work, and an automated solution is therefore preferable. By performing the scan automatically, time is saved during the scanning process, and the resulting spatial map of LEED patterns can be investigated in ways that are not possible otherwise. For example, small regions of high quality may be located which would have been missed during manual operation, and valuable information about variations in crystal quality or ordering may become apparent.

To support automated user-configurable LEED raster scanning, new control software was developed, which can be seen in Fig. 10. The software interfaces directly with both the mechanical controls and the camera, allowing the user to manually move around the surface plane while observing the live feed of the LEED pattern. Movement is bounded within a configurable area to prevent crashing into the LEED instrument or other physical objects within the chamber. The configuration of the area is normally done a single time for a given LEED instrument since it is a function of the contents of the chamber and size of sample holders.

The main feature of the software is to perform an automated scan across the sample, which can either be initiated for the whole area or for a subsection. During a scan, a raster movement will be performed using a vertical and horizontal step size chosen by the user, and a picture will be saved at each point after waiting for the duration of the camera exposure. Other than making sure the LEED instrument itself is not located too close to the sample holder, a scan can be safely left unsupervised, provided that the configuration of the scan area has been performed properly.

Additionally, the serial protocol for interfacing with the LEED controller was reverse engineered and implemented in order to take full control of the LEED setup and allow for other applications such as automated scans at different beam energies. For the measurements presented in this study, the LEED settings were kept constant.

4.3 Analysis

Raster scanning has already been applied at the Bloch beamline for ARPES measurements, and interactive software exists for analysing the results. Although this tool was developed for investigation of ARPES spectra, most functionality is based purely on the raw image data, which works equally well for LEED images. It was therefore possible to perform the primary analysis without any changes to the software. The tool allows visualization of total intensity across a 2D data set and comparison of relative intensities of two areas. The sharpness of intensity peaks can also be analyzed at a chosen cross-section of the image, and view how it compares to sharpness in the same area across the sample. The sharpness analysis is currently performed in a rudimentary way, which is a result of reusing previous tooling. No specific peak model is used, and instead the selected

region is averaged, smoothed and the derivative computed. The resulting derivative is then smoothed again, and the largest value of the second derivative is reported. This approximates sharpness detection, while not making prior assumptions about number of peaks in the image or their positions.

Reusing an existing analysis software was not entirely optimal, and there are limitations in the insight that can be acquired just from intensity comparisons and rudimentary sharpness detection. For our use cases the results were mostly satisfactory, and the only noticeable practical issue was the drift of LEED spots across images. The drift was likely caused by a slight distortion of the electron beam, due to a faulty manipulator. When analysing the scan, drifting translates into a difficulty in isolating areas of interest, requiring larger areas of integration when analysing spot intensities across the map.

5 Results: SiC on TaC and small crystal cleaving

The results of LEED raster scans of two categories of samples are presented. Inhomogeneity is investigated in monolayer SiC on TaC, and localization of small areas of sharp LEED patterns is done on a single cleaved crystal of $PtTe_2$ as well as an array of multiple cleaved arbitrary crystals.

5.1 SiC on TaC

The sample, during annealing, is presented in Fig. 11a. An intensity map based on total intensity of LEED images can be seen in Fig. 11(b-c). Large agreement between the outline captured by the LEED scan and the physical sample is observed. Upon closer inspection, the top corner in the LEED outline is obstructed by the clamp as expected, but the bottom corner presents dark areas which are seemingly correlated with the hot spot seen in Fig. 11a.

5.1.1 Graphene layers

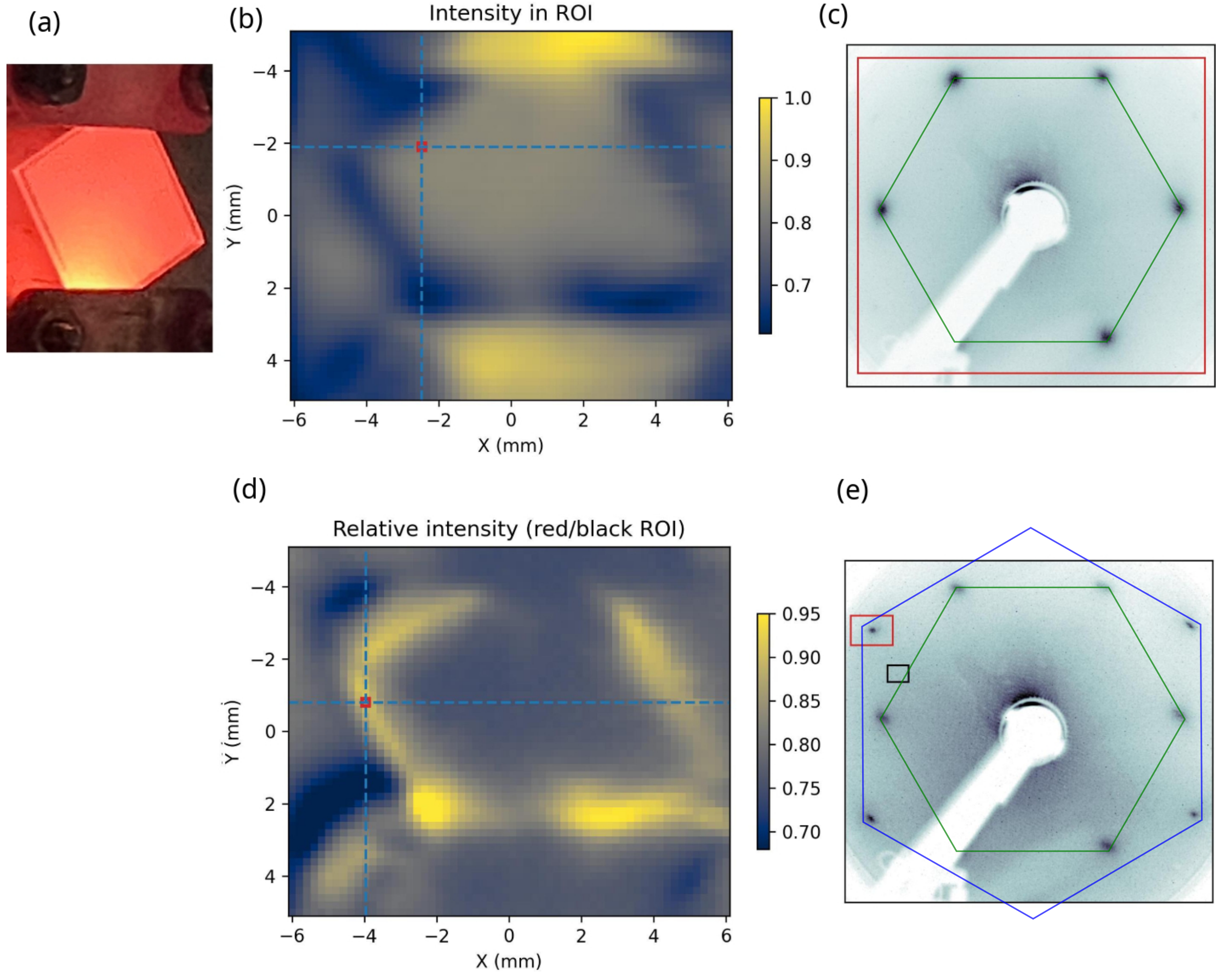

FIG. 11: LEED raster scans of the SiC-on-TaC sample. **(a)** Photograph of the SiC-on-TaC sample during annealing. Notably, the clamps cover part of the sample, and a heat gradient is observed with a significant hot-spot in one corner. Most of the sample is covered by a thin layer of TaC on top of SiC, but along the edges there is uncovered bulk SiC. **(b)** Plot of total intensity of entire LEED image. Since a clear LEED pattern is produced across the whole surface, an outline of the sample in the intensity map is observed. **(c)** LEED image at location indicated in (b), where the hexagonal LEED pattern expected from SiC is observed. **(d)** Relative intensity comparison between graphene LEED pattern and background. **(e)** LEED image where an additional graphene pattern can be seen.

The study on growth of monolayer SiC [3], for which the sample was originally produced, outlined expectations of graphene formation on the sample. Graphene was expected along the edges due to non-total coverage of TaC, and in one corner due to non-uniform heating during annealing. The results from a LEED scan, presented in Fig. 11(d-e), confirms these expectations, with a clear outline around the edges and a strong response in the

bottom corner. From this, it was concluded that excessive heating in the lower area during annealing has turned surface layer SiC into graphene, similarly to the uncovered bulk SiC along the edges.

To further verify the results, an XPS raster scan was performed on the same sample, at 440 eV photon energy. A spectra of C 1s peaks, known from the previous work, is shown in Fig. 12a and can be used to interpret the XPS measurements. By selecting a spectra at a location on the sample and focusing on a single peak, a contrast map can be generated, showing regions where that particular peak is prevalent. Fig. 12(b-c) highlights the region matching the bilayer graphene peak, while Fig. 12(d-e) shows the region rich in honeycomb SiC. The resulting spatial maps are in good agreement with the LEED maps presented in Fig. 11, confirming the utility of the LEED raster scanning technique. It should however be noted that XPS, being a much more precise technique, gives higher resolution and will contain information not present in a LEED scan. For example, in Fig. 12c, small spots of graphene can be seen across the sample ,which are not detected by LEED due to limited spatial resolution.

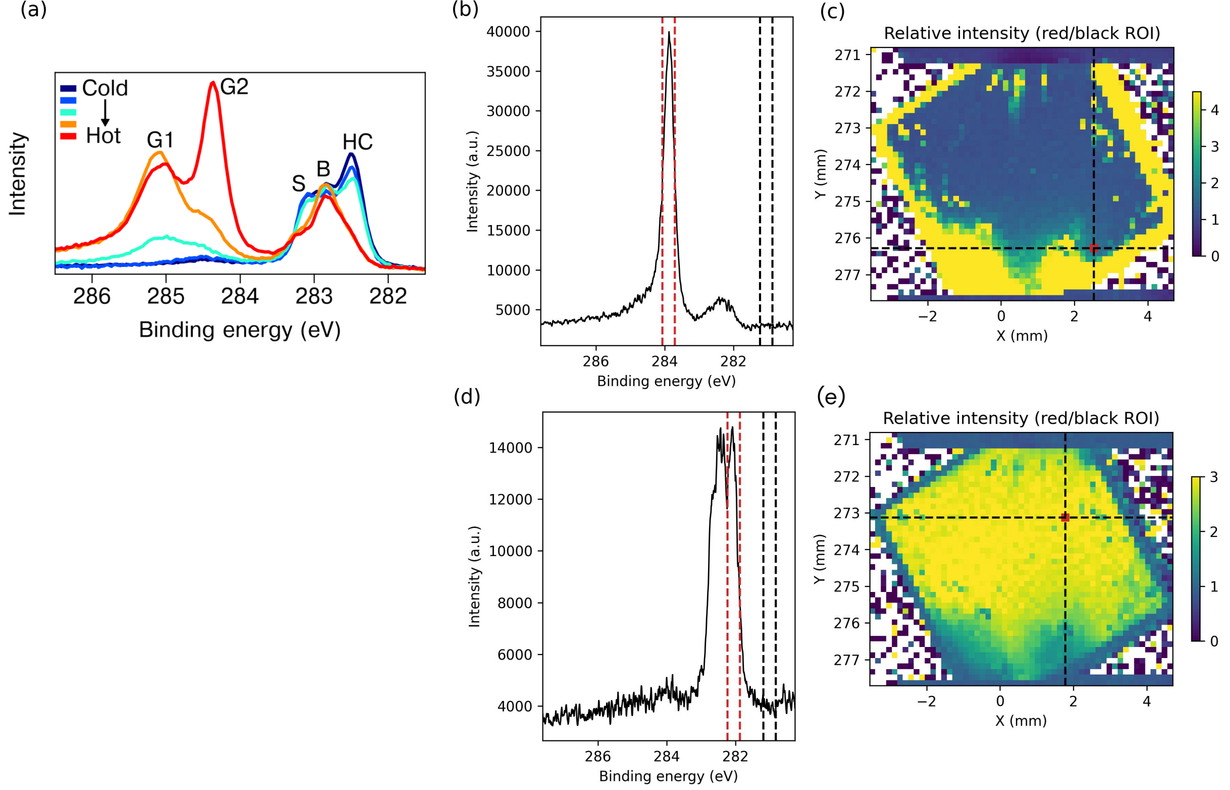

FIG. 12: **(a)** C 1s x-ray photoelectron spectra of SiC-on-TaC sample recorded during the original study [3], based on the temperature gradient across the sample during annealing. G1 and G2 levels correspond to monolayer and bilayer graphene, while HC corresponds to monolayer honeycomb SiC. S and B peaks are surface and bulk carbon, but they are not relevant for the analysis performed in this study. **(b)** XPS measurement at the location indicated in (c). The peak marked in red corresponds to the C 1s binding energy of bilayer graphene. **(c)** Intensity map of the peak highlighted in red in (b), relative to the background region highlighted in black. **(d)** XPS measurement at the location indicated in (e). The peak marked in red corresponds to the C 1s binding energy of honeycomb SiC. **(e)** Intensity map of the peak highlighted in red in (d), relative to the background region highlighted in black.

5.1.2 Inhomogeneity of monolayer SiC

An intensity map of the SiC-on-TaC LEED scan is presented in Fig. 13a, which reveals that the monolayer SiC is not fully homogeneous across the surface, with the central region showing a weaker signal. This inhomogeneity of the monolayer SiC was not previously known, and is a direct result of investigating the sample using a raster scanning technique. The lattice symmetry is therefore higher in the side regions, which means these regions contain the most well-formed crystal structure. A supplementary ARPES scan across the sample is shown in Fig. 14, together with spectra at two locations, side and centre, of the

sample. Upon inspection of the energy bands, the central region presents a broader and lower intensity signal, which is in agreement with the LEED scan.

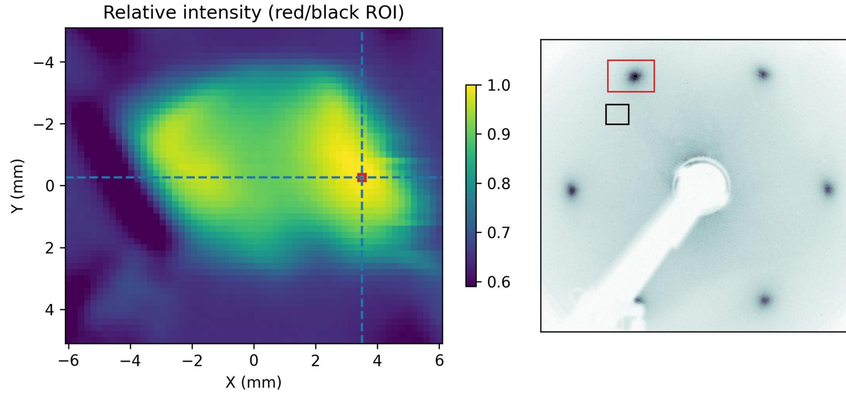

FIG. 13: Intensity analysis of monolayer SiC LEED pattern relative background. The central region shows weaker intensity. The red and black rectangles indicate regions of integration for signal and background, respectively.

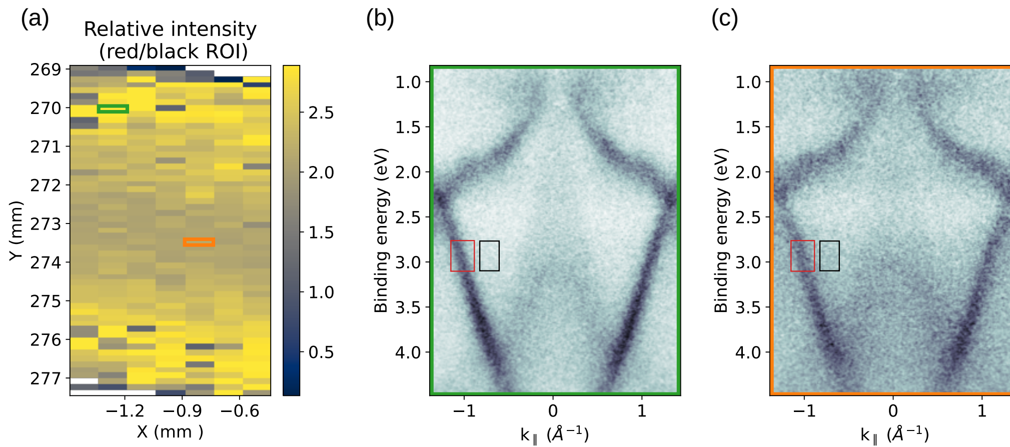

FIG. 14: **(a)** Intensity analysis of ARPES scan across the SiC-on-TaC sample, at 100 eV photon energy, where the central region shows lower intensity. The spectra in (b) and (c) are located at the green and orange spots, respectively, and the red and black rectangles show the areas of integration for signal and background. **(b)** ARPES image at top/green location in (a), with high-intensity and sharp spectrum. **(c)** ARPES image at central/orange location in (a), with weaker and less sharp spectrum.

5.2 Small crystal ($PtTe_2$)

A $PtTe_2$ crystal was investigated by means of LEED raster scanning, with the intention of locating a spot where a well-formed surface structure can be observed. An initial coarse

scan, at 0.5 mm step size, is presented in Fig. 15a where a region of high intensity signal can be seen. A LEED image at a location within the high-intensity region is presented in Fig. 15b, where a weak and unclear LEED pattern can be seen.

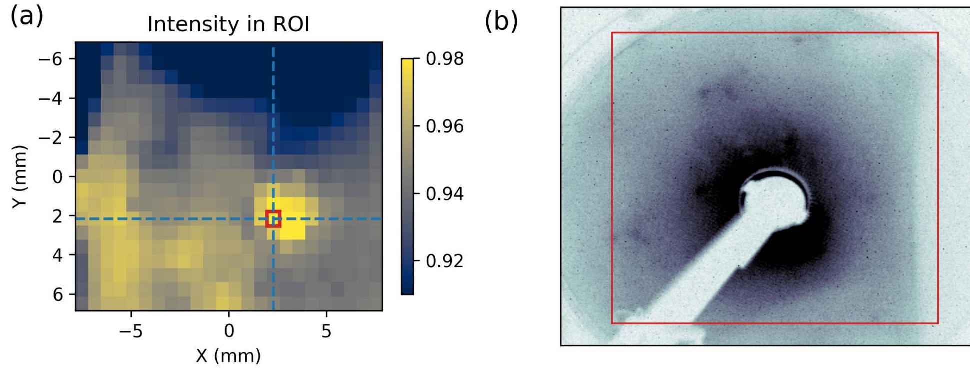

FIG. 15: Raster LEED scan with large step length of 0.5 mm across entire $PtTe_2$ sample. Total intensity is used to identify which area of the sample might produce LEED patterns.

A secondary scan was performed in the high intensity region with a much smaller step size of 0.1 mm. By manually scrubbing around the resulting 2D image, a location with a higher intensity, but still blurry, LEED pattern was found. Analyzing the sharpness of the highest-intensity spot revealed a secondary region with similar sharpness, which can be seen in Fig. 16a. Scrubbing around the region and observing the LEED images by eye, a location with a sharp LEED pattern was quickly found, as seen in Fig. 16b. In order to verify that the location found through this process presents the clearest LEED pattern on this sample, all LEED images were manually inspected, and no other location was found to have a better LEED pattern. We therefore conclude that the usage of LEED raster scanning is a viable and quick method of locating regions of well-formed crystal surface, if they exist.

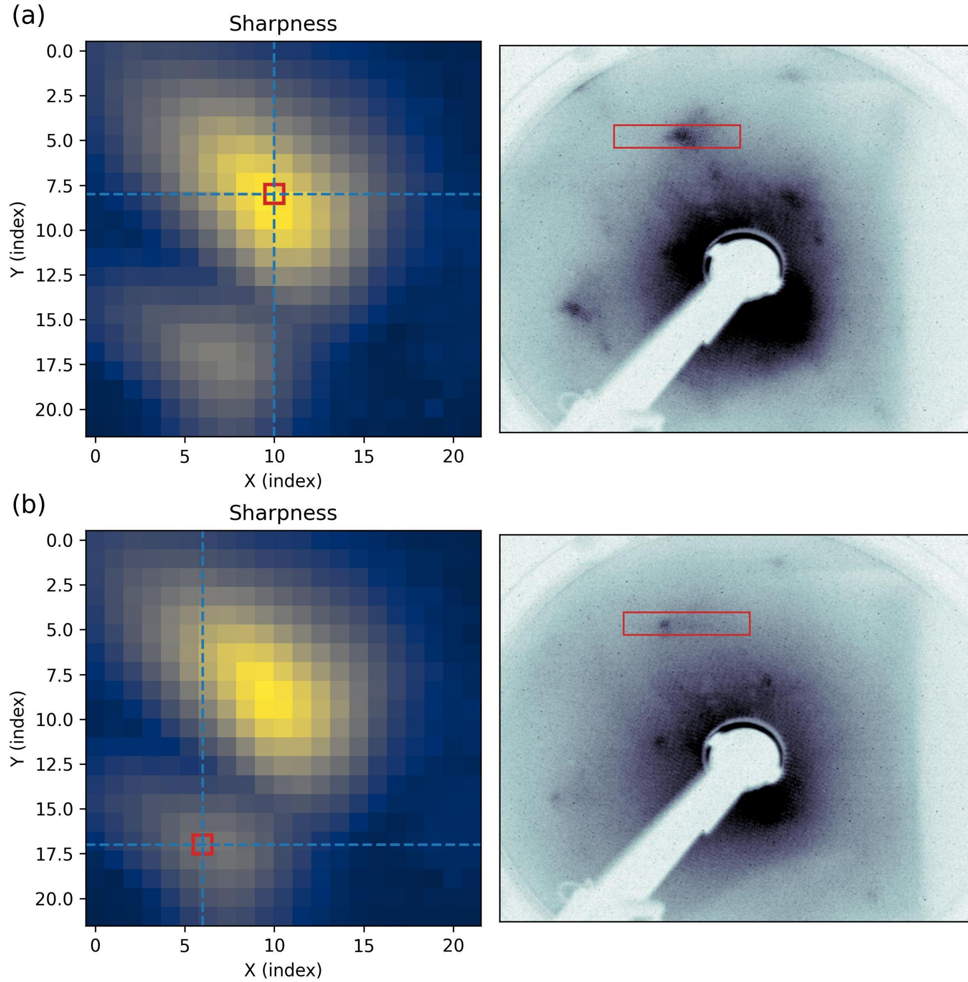

FIG. 16: Sharpness analysis of the fine scan over the region identified in Fig. 15. **(a)** Shows a location in the fine scan, indicated by the cross-hair in the left image. Blurry LEED spots are observed in the LEED image at this location, and the area to integrate over for sharpness analysis is chosen, indicated by the red rectangle around one spot. **(b)** Secondary location, picked by moving to the lower-left region of the scan, highlighted by similarity in sharpness. Sharper spots are seen in the LEED image on the right.

5.3 Multiple cleaved samples

A final study was performed with four crystals on a single sample holder, as depicted in Fig. 9. A LEED scan was taken at step size 0.2 mm, primarily in the horizontal direction, producing the intensity map shown in Fig. 17. The results indicate that neither crystal cleaved well, and only the left-most sample produced anything resembling a LEED pattern. Still, the method shows that areas with some level of LEED response can be highlighted through a quick scan and, based on the prior result with the $PtTe_2$ crystal, we find it plausible that the method would have located a LEED signal maxima if sites

with well-formed surface structure were present. Current results do not indicate the level of trust that can be given when finding good cleaving sites using LEED scanning, but we believe a repeat study would show promise also in the multiple-samples case.

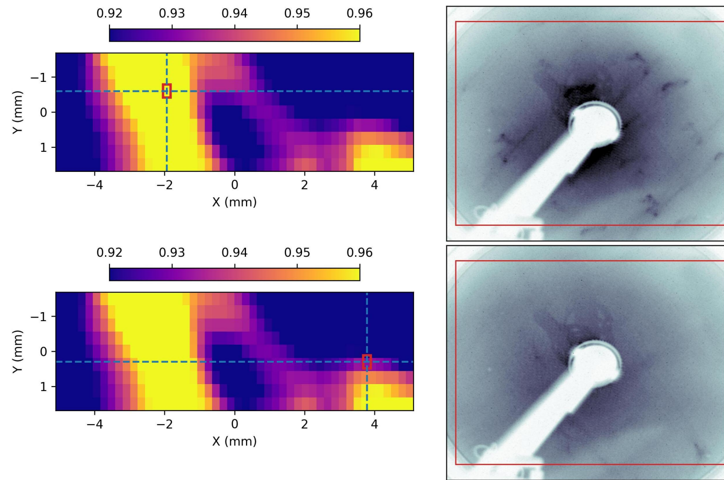

FIG. 17: Intensity map of LEED raster scan across multiple top posted samples. Neither sample has cleaved well, but regions corresponding to diffraction response can clearly be seen. Exploring a highlighted region simplifies the process of finding a well-cleaved location if one exists, which is hinted at in the upper image.

6 Conclusion

We have demonstrated the use of a LEED instrument in a raster scanning fashion for the purpose of classifying the quality of samples and verifying expectations from the preparation process. The work was inspired by previous usage of ARPES for raster scanning, and upon comparison we found good correlation between the two methods in mapping of inhomogeneity. Additionally, previously unknown information of lower sample quality in the central region of the SiC-on-TaC sample was clearly seen from the LEED scans. This had been missed in the original study [3], where only specific locations of the sample were measured.

Seen purely from a quantitative standpoint, LEED raster scanning produces less detailed results than advanced surface sensitive techniques such as ARPES or Photo-Emission Electron Microscopy (PEEM). When costs in time and complexity are taken into account, however, there are compelling arguments for using LEED scanning in situations where the results provide adequate information. The LEED raster scans taken during this study

were performed by a single person without prior experience in experimental work after a short introduction to the setup, and the duration of each scan was less than one hour. In contrast, the ARPES scan taken of the same sample was performed by a person with expert knowledge of the system and, more importantly, required ten hours of beamtime. For the purpose of inhomogeneity mapping, the only information present exclusively in the XPS scan were a small number of tiny graphene spots across the sample. Hence we conclude that LEED raster scanning can be an immensely useful tool during sample preparation, being low-cost both in time and money. For samples where successful cleaving proves difficult, such as the one presented Fig. 1, a quick and low-complexity method for investigating the quality of cleaved surfaces prior to beamline access allows for more time spent gathering data rather than localization of measurement sites. In general, we believe there is high value in a fast and low-barrier method for verifying expectations of a sample, filtering out the low end such as bad cleaves and accidental inhomogeneity, prior to moving forward in the experimental process. We believe LEED raster scanning is very suitable for this task.

7 Outlook

The results in this study were analyzed using previously existing software developed for ARPES raster scans, with the primary available tool being intensity comparison. By developing specific analysis tools for LEED scans, data presentation would be clearer and more insights could be gained. A primary issue faced during our analysis was drift of LEED patterns across measurement locations, most likely caused by distortion of the electron beam due to a faulty manipulator. The issue of drifting spots presents itself as increased areas of integration for each LEED spot, making comparative intensity analysis across the sample difficult and inexact. By moving from pixel-level comparisons to identification of individual spots in each LEED picture, the issues of drifting can be further mitigated. Each spot can then be analyzed for intensity and sharpness and compared across locations in a direct manner, giving much cleaner data presentation.

During the study, work was also done allowing automatic control of the parameters of the LEED controller. This functionality was not used during our measurements, however further studies could expand into doing two-dimensional LEED IV-spectra, by running

scans across the sample at different beam energies.

References

[1] K. S. Novoselov, A. K. Geim, S. V. Morozov, D. Jiang, Y. Zhang, S. V. Dubonos, I. V. Grigorieva, and A. A. Firsov. Electric Field Effect in Atomically Thin Carbon Films. *Science*, 306:5696, 2004. doi:10.1126/science.1102896.

[2] Ed Gerstner. Nobel Prize 2010: Andre Geim & Konstantin Novoselov. *Nature Physics*, 6:11, 2010. doi:10.1038/nphys1836.

[3] C. M. Polley, H. Fedderwitz, T. Balasubramanian, A. A. Zakharov, R. Yakimova, O. Bäcke, J. Ekman, S. P. Dash, S. Kubatkin, and S. Lara-Avila. Bottom-Up Growth of Monolayer Honeycomb SiC. *Physical Review Letters*, 130:076203, 2023. doi:10.1103/PhysRevLett.130.076203.

[4] M. Houmad, O. Dakir, A. Abbassi, A. Benyoussef, A. El Kenz, and H. Ez-Zahraouy. Optical properties of SiC nanosheet. *Optik*, 127:4, 2016. doi:10.1016/j.ijleo.2015.11.017.

[5] Xiao Lin, Shisheng Lin, Yang Xu, Ayaz Ali Hakro, Tawfique Hasan, Baile Zhang, Bin Yu, Jikui Luo, Erping Li, and Hongsheng Chen. Ab initio study of electronic and optical behavior of two-dimensional silicon carbide. *Journal of Materials Chemistry C*, 1:2131–2135, 2013. doi:10.1039/C3TC00629H.

[6] Sakineh Chabi and Kushal Kadel. Two-Dimensional Silicon Carbide: Emerging Direct Band Gap Semiconductor. *Nanomaterials*, 10:2226, 2020. doi:10.3390/nano10112226. URL `https://www.mdpi.com/2079-4991/10/11/2226`.

[7] S. S. Lin. Light-emitting two-dimensional ultrathin silicon carbide. *The Journal of Physical Chemistry C*, 116:6, 2012. doi:10.1021/jp210536m.

[8] Rovi Angelo B. Villaos, Christian P. Crisostomo, Zhi-Quan Huang, Shin-Ming Huang, Allan Abraham B. Padama, Marvin A. Albao, Hsin Lin, and Feng-Chuan Chuang. Thickness dependent electronic properties of Pt dichalcogenides. *npj 2D Materials and Applications*, 3:2, 2019. doi:10.1038/s41699-018-0085-z.

[9] Meng-Kai Lin, Rovi Angelo B. Villaos, Joseph A. Hlevyack, Peng Chen, Ro-

Ya Liu, Chia-Hsiu Hsu, José Avila, Sung-Kwan Mo, Feng-Chuan Chuang, and T.-C. Chiang. Dimensionality-Mediated Semimetal-Semiconductor Transition in Ultrathin $PtTe_2$ Films. *Physical Review Letters*, 124:036402, 2020. doi:10.1103/PhysRevLett.124.036402.

[10] Longhui Zeng, Di Wu, Jiansheng Jie, Xiaoyan Ren, Xin Hu, Shu Lau, Yang Chai, and Yuen Tsang. Van der Waals Epitaxial Growth of Mosaic-Like 2D Platinum Ditelluride Layers for Room-Temperature Mid-Infrared Photodetection up to 10.6 µm. *Advanced Materials*, 32:2004412, 2020. doi:10.1002/adma.202004412.

[11] G. Attard and C. Barnes. *Surfaces*, chapter 2.3 Low energy electron diffraction (LEED). Oxford Chemistry Primers. Oxford University Press, 2011. ISBN 9780191848964.

[12] Ponor, CC BY-SA 4.0 (https://creativecommons.org/licenses/by-sa/4.0), via Wikimedia Commons, . URL `https://commons.wikimedia.org/wiki/File:Low-energy_electron_diffraction_(LEED)_instrument_-_schematic_diagram.svg`. Accessed April 4, 2024.

[13] Antoine Kahn. Fermi level, work function and vacuum level. *Journal of Materials Chemistry C*, 3:7–10, 2016. doi:10.1039/C5MH00160A.

[14] Baiqing Lv, Tian Qian, and Hong Ding. Angle-resolved photoemission spectroscopy and its application to topological materials. *Nature Reviews Physics*, 1:10, 2019. doi:10.1038/s42254-019-0088-5.

[15] Jonathan A. Sobota, Yu He, and Zhi-Xun Shen. Angle-resolved photoemission studies of quantum materials. *Reviews Of Modern Physics*, 93:025006, 2021. doi:10.1103/RevModPhys.93.025006.

[16] Ponor, CC BY-SA 4.0 (https://creativecommons.org/licenses/by-sa/4.0), via Wikimedia Commons, . URL `https://upload.wikimedia.org/wikipedia/commons/7/70/Electron_spectrometer_for_ARPES%2C_working_principle.svg`. Accessed May 3, 2024.

[17] Ponor, CC BY-SA 4.0 (https://creativecommons.org/licenses/by-sa/4.0), via Wikimedia Commons, . URL `https://upload.wikimedia.org/wikipedia/commons/3/3f/ARPES_analyzer_cross_section.svg`. Accessed May 3, 2024.

[18] The Bloch beamline team. Beamline Review Report. 2022. URL https://www.maxiv.lu.se/beamlines-accelerators/beamlines/bloch/. Accessed April 18, 2024.